NeuroImage: Clinical 29 (2021) 102563

Contents lists available at ScienceDirect

NeuroImage: Clinical

journal homepage: www.elsevier.com/locate/ynicl

Evaluating transcranial magnetic stimulation (TMS) induced electric fields in pediatric stroke

Kathleen E. Mantell [a], Ellen N. Sutter [b], Sina Shirinpour [a], Samuel T. Nemanich [b], Daniel H. Lench [b], Bernadette T. Gillick [b], Alexander Opitz [a,*]

[a] Department of Biomedical Engineering, University of Minnesota, Minneapolis, USA
[b] Department of Rehabilitation Medicine, University of Minnesota, Minneapolis, USA

A B S T R A C T

Transcranial magnetic stimulation (TMS) is an increasingly popular tool for stroke rehabilitation. Consequently, researchers have started to explore the use of TMS in pediatric stroke. However, the application of TMS in a developing brain with pathologies comes with a unique set of challenges. The effect of TMS-induced electric fields has not been explored in children with stroke lesions. Here, we used finite element method (FEM) modeling to study how the electric field strength is affected by the presence of a lesion. We created individual realistic head models from MRIs (n = 6) of children with unilateral cerebral palsy due to perinatal stroke. We conducted TMS electric field simulations for coil locations over lesioned and non-lesioned hemispheres. We found that the presence of a lesion can strongly affect the electric field distribution. On the group level, the mean electric field strength did not differ between lesioned and non-lesioned hemispheres but exhibited a greater variability in the lesioned hemisphere. Other factors such as coil-to-cortex distance have a strong influence on the TMS electric field even in the presence of lesions. Our study has important implications for the delivery of TMS in children with brain lesions with respect to TMS dosing and coil placement.

1. Introduction

Ischemic perinatal stroke affects as many as 1 in 2700 live births and can result in lifelong burden of care for both individuals and their families (Agrawal et al., 2009). Rehabilitation techniques that promote functional recovery are indicated to improve quality of life for individuals with stroke. Transcranial magnetic stimulation (TMS) has shown promise as a noninvasive cortical assessment and neuromodulation technique for stroke rehabilitation in adult populations (Emara et al., 2010; Lindenberg et al., 2010; Ridding and Rothwell, 2007), although with varied outcomes amongst studies (Malcolm et al., 2007; Theilig et al., 2011; Wiethoff et al., 2014). Increasingly, researchers are exploring TMS as a rehabilitation option for pediatric populations (Gillick et al., 2018, 2014; Kirton et al., 2008). These efforts, however, come with additional challenges due to variations in anatomy and function in the developing brain affected by brain injury. In particular, it is not clear if and how TMS dosing has to be adjusted for a pediatric population affected by brain injury (Rossi et al., 2009). Electric field modeling based on individually realistic head models has proven itself to be a promising tool to guide TMS applications (Aberra et al., 2020; Bungert et al., 2016; Gomez–Tames et al., 2020; Gomez-Tames et al., 2018; Goodwin and Butson, 2015; Opitz et al., 2016, 2014, 2013, 2011).

Current clinical practice for stroke rehabilitation with repetitive TMS (rTMS) typically involves either excitatory stimulation of motor areas of the affected hemisphere or inhibitory stimulation of the unaffected hemisphere (Dionísio et al., 2018; Hoyer and Celnik, 2011). A key parameter for rTMS is to select the stimulation intensity which varies across different clinical trials. As the TMS electric field is affected by the conductivities of various brain/head tissues, in particular cerebrospinal fluid (CSF), the presence of lesions can affect TMS dosing. In this study, we aim to characterize the TMS electric fields in the presence of cortical or subcortical lesions and compare them to corresponding targets in the unaffected hemisphere.

Modeling studies have highlighted the importance of the interface between gray matter (GM) and cerebrospinal fluid (CSF) strongly impacting the TMS induced electric fields (Miranda et al., 2003; Thielscher et al., 2011). Therefore, in the presence of brain lesions with varying size and location, TMS electric fields will differ in their strength and spatial extent. These variations likely contribute to the variability in clinical outcomes observed in TMS for stroke rehabilitation.

Few studies have explored the impact of brain lesions on TMS-induced electrical effects so far. Two previous studies used computational modeling in adult stroke. The first detected the TMS-induced current density was greatly affected by the presence of a lesion (Wagner et al., 2006). The second found comparable TMS electric field

* Corresponding author.
E-mail address: aopitz@umn.edu (A. Opitz).

https://doi.org/10.1016/j.nicl.2021.102563
Received 13 July 2020; Received in revised form 7 January 2021; Accepted 8 January 2021
Available online 13 January 2021

strength between lesioned and non-lesioned brains (Minjoli et al., 2017) with additional anatomical factors likely influencing the electric field distribution. However, it is not clear how these findings in adults apply in pediatric stroke and across a range of different lesion locations and types (cortical vs subcortical). Our study goes beyond previous work (Minjoli et al., 2017) by investigating a pediatric population and in a larger sample (n = 6). Further, we perform additional analyses of TMS electric field components and statistical analyses of the effects determining the electric fields in affected and unaffected hemispheres. We comprehensively evaluate and compare electric fields between lesioned and non-lesioned hemispheres and identify key factors determining the electric field distributions. These efforts can help understand how lesion sizes and locations due to perinatal stroke affect the TMS induced electric field in the brain. This will facilitate future studies to utilize individual realistic head models to identify stimulation targets and dosing parameters for synergistic neuromodulation and rehabilitation interventions.

2. Methods

2.1. Participants

MR images from six participants (8–19 years, 3 female) with imaging-confirmed perinatal stroke and a clinical diagnosis of resultant unilateral cerebral palsy were used in this study. Participants were recruited as part of a larger study (NCT# 02250092) incorporating MRI, non-invasive brain stimulation, and behavioral training. Inclusion criteria required the presence of an MEP from both hemispheres as assessed by TMS. Exclusion criteria included seizures within the past two years, implanted metal or medical devices contraindicated for MRI or brain stimulation, co-occurring disorders or medical condition (e.g., brain injury, neoplasm, and pregnancy), communication deficits preventing responding to safety questions, or a history of phenol or botulinum toxin injections within the past 6 months. MR images were collected with approval from the University of Minnesota Institutional Review Board. All participants ages 18 years and older and caregivers of children ages 7–17 provided consent after informed consent discussion. All children ages 7–17 provided assent.

Table 1 summarizes information about the lesion locations and type for each participant. Here we define a cortical lesion as a lesion that breaches the cortical surface, even though it may also affect subcortical structures. In contrast, a subcortical lesion is defined as a lesion that is completely contained inside the brain without touching the outer surface.

2.2. MR image parameters

MRI scans were performed at the University of Minnesota Center for Magnetic Resonance Research on a 3-Tesla Prisma scanner (Siemens Inc., Erlangen, Germany) using a 32-channel head coil. T1 images were acquired with an MPRAGE sequence (176 sagittal slices with 1 mm isotropic voxels, flip angle = 7°, TR/TE/TI = 2530/3.65/1100 ms). Images for each participant showing the lesion location can be found in supplementary Fig. 1.

Table 1
Participant demographic and lesion information: Age, sex, side and location of the lesion, and how many TMS coil positions were needed to cover the lesion.

ID	Age	Sex	Lesion Side		Lesion Location		Simulations per Hemisphere
			Left	Right	Cortical	Subcortical	
P1	8	M	X		X		140
P2	15	F	X		X		153
P3	14	F	X			X	221
P4	19	F		X	X		96
P5	12	M		X		X	187
P6	8	M	X			X	135

2.3. Head model generation

We generated morphologically accurate tetrahedral head meshes for each of the six participants. We used the SimNIBS head model generation pipelines, mri2mesh (Windhoff et al., 2013) and headreco (Nielsen et al., 2018) to produce initial automated segmentation masks for white matter (WM), gray matter (GM), cerebrospinal fluid (CSF), skull, and skin. Since mri2mesh and headreco are designed to segment MR images for typical healthy adults, we manually corrected these initial segmentation masks for any errors, particularly in GM and WM. Further, we manually segmented lesions based on the T1 image for each individual using ITK-SNAP (Yushkevich et al., 2006); lesions were segmented by five researchers and thresholded to include only voxels which at least 3 of 5 researchers included in the segmentation. After all the segmentation masks were updated, we integrated the lesion mask using fslmaths (Jenkinson et al., 2012). Cortical lesion masks (on the surface of the brain) were subtracted from the GM and WM masks. Subcortical lesion masks connected to the ventricles were added to the ventricle mask. We then converted the masks into surfaces and decoupled them using meshfix (Attene, 2010). Since SimNIBS uses surface-based meshing, decoupling was executed from the inside out to ensure complete nesting of the surfaces. The nesting required a thin layer of GM coating the inside of the lesion. The resulting head models had $5.5 \times 10^5 - 7.7 \times 10^5$ triangles and $2.3 \times 10^6 - 3.1 \times 10^6$ tetrahedra. An example of the final segmentation masks and resulting FEM head model is shown in Fig. 1. Additional details about the meshing process can be found in the supplementary materials.

2.4. FEM simulations

All simulations were run using SimNIBS v3.0.5. To estimate the impact of TMS over lesioned vs non-lesioned brain areas, we conducted simulations for multiple TMS coil locations. For this, we set up TMS locations on a grid (10 mm spacing between points) spanning lesioned and non-lesioned brain regions (Fig. 2A + B). Depending on lesion size and location, the number of simulation positions varied from model to model, ranging from 96 to 221 positions per hemisphere (see Table 1). For cortical lesions the grids were large enough to cover the entire lesion and surrounding intact tissue. As there were no surface landmarks to distinguish between positions over the lesion and over intact cortical tissue, subcortical lesion grids covered most of the hemispheres. We further mirrored the grid onto the non-lesioned hemisphere to allow comparisons of electric fields between lesioned and non-lesioned sides. We set the coil to standard motor orientation, 45° to the longitudinal fissure, for all positions (Fig. 2C). We performed simulations for a Magstim 70 mm figure-of-eight coil file included in the SimNIBS package ($dI/dt = 1 \times 10^6$ A/s) to solve for the induced electric field strength at each coil grid position (Fig. 2D + E).

TMS simulations were performed using realistic conductivity values for each tissue type ($\sigma_{skin} = 0.465$ S/m, $\sigma_{bone} = 0.01$ S/m, $\sigma_{CSF} = 1.654$ S/m, $\sigma_{GM} = 0.275$ S/m, and $\sigma_{WM} = 0.126$ S/m (Windhoff et al., 2013)). In addition, we reran all simulations and analyses with a 25 mm coil, used previously in (Alekseichuk et al., 2019) and for a second coil orientation (135°).

2.5. Data analysis

Electric field simulation results were analyzed using custom MATLAB (MathWorks, Natick, MA) scripts. During the analysis, we excluded TMS grid positions (<8% per participant) that were not directly located over the brain surface (e.g. too inferior) or practically not accessible (e.g. too close to the eyes).

As a first step, we evaluated the electric field strength for each coil location and compared lesion to non-lesion sites. We defined the

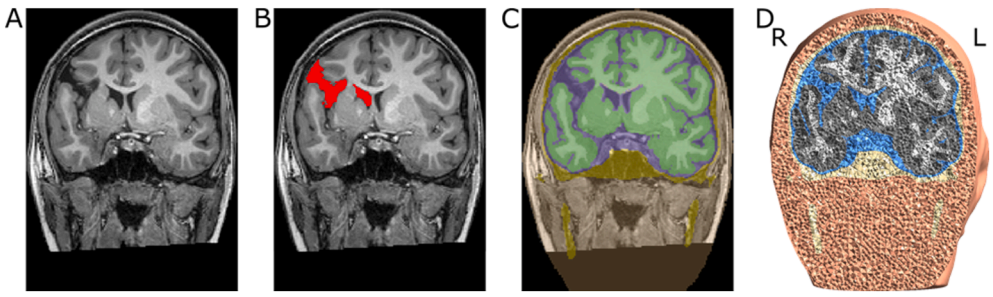

Fig. 1. Illustration of FEM head model creation. A) Anatomical T1-weighted MR image. B) Manually generated lesion mask. C) Final segmentation masks including skin (orange), skull (yellow), CSF (blue), GM (dark green), and WM (light green). Masks were generated by using automated segmentation routines from SimNIBS, then combined with hand segmented lesion masks, and manually corrected. D) Final 3D FEM head model showing volume tetrahedra for the different tissue types (skin (orange), skull (yellow), CSF (blue), GM (gray), WM (white). (For interpretation of the references to colour in this figure legend, the reader is referred to the web version of this article.)

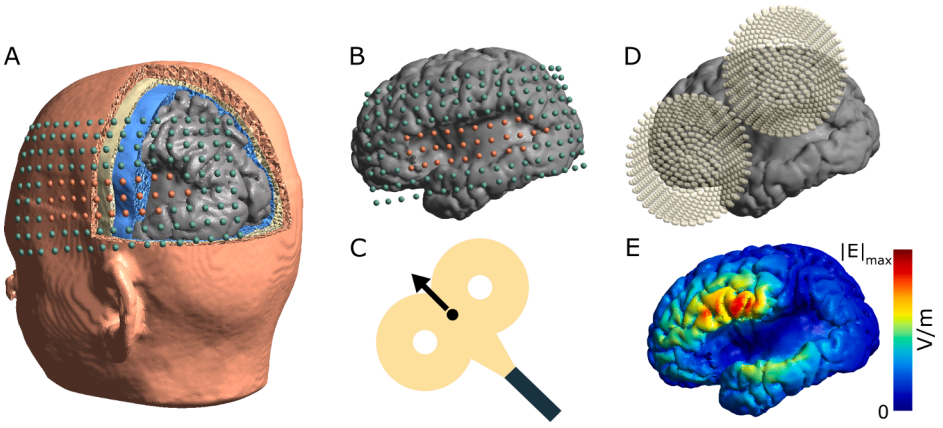

Fig. 2. Overview of TMS simulations A) The grid of simulated TMS coil positions shown on the 3D head model's skin surface. Simulations were performed with a 4 mm distance between the skin and the coil center. B) Simulation grids were individually centered on the lesion. Orange spheres indicate positions directly over the lesion; green spheres indicate positions not over the lesion. C) The center of the coil (black dot) corresponds to the spheres shown in A) and B). The TMS coils are oriented 45° to the midsagittal plane. D) Example TMS coil location and orientation for one TMS simulation. E) Resulting TMS induced electric field strength shown in the GM surface for the coil position in D). (For interpretation of the references to colour in this figure legend, the reader is referred to the web version of this article.)

affected surface area as that including all GM triangles whose electric field strength is greater than or equal to 50% of the robust maximum (99.9th percentile) of the electric field strength for a given coil position. We chose a 50% threshold according to current practice in the field (Deng et al., 2013; Thielscher et al., 2011) and to allow easy comparison to other modeling studies. In case of the presence of large cortical lesion this will lead to affected brain areas at the periphery of the lesion volume. Thus, care has to be taken when interpreting the results for the two patients with extended lesions (P1 and P2) to the unaffected hemisphere. We then determined the mean electric field strength as the mean of the affected surface area of GM. For each individual, all mean electric field strengths were divided by the maximum mean electric field strength across all coil positions for that individual. This normalization allows us to compare across individuals without taking into account additional factors, such as age, sex, head size, etc.

Secondly, we sought to identify anatomical and procedural factors on the TMS induced electric fields. In particular, we evaluated the effect of coil-to-cortex distance, CSF depth, CSF volume, and mean local curvature on the TMS electric field. We defined coil-to-cortex distance as the Euclidian distance between the TMS coil center and the closest GM triangle. We determined the local CSF depth by projecting the coil center onto the CSF surface and averaging the distance between that point and the center of every GM triangle within a 1.0 cm radius, 10.0 cm height cylinder after the models were sliced to exclude triangles from the opposite hemisphere. We calculated CSF volume by summing the volume of all CSF tetrahedra whose centers were within the same cylinder and modeling slicing used for determining the CSF depth. Mean local curvature describes how much the brain surface curves away from the TMS coil. The curvature of the CSF surface is used here as a proxy measurement for how much the brain underneath it curves without the gyri curvature affecting the value. This was calculated by smoothing the CSF surface 20 times using mris_smooth from FreeSurfer (Fischl, 2012) and then averaging the node curvatures within a 2.0 cm radius circle centered at each coil position.

To quantify the effects of these factors (coil-to-cortex distance, CSF depth, CSF volume, and mean local curvature) we calculated one- and two-factor linear models ($y \sim 1 + x_1 + x_2$, where y = mean |E| and x_i = factor(s) included in the model) separately for each hemisphere of each participant.

3. Results

3.1. TMS induced electric fields

We ran simulations using realistic tissue conductivities. In an homogeneous model, the electric field strength decreases purely with distance from the coil, whereas in the realistic model enhanced electric field strengths occur at tissues boundaries (Opitz et al., 2011) due to the changes in conductivity (Fig. 3).

We averaged the normalized electric field strength for each coil position on the lesioned hemisphere and for each position on the non-lesioned hemisphere for each participant. We found that across participants, there was no difference between hemispheres in average electric field strength (lesioned hemisphere E_{mean} = 0.8870 ± 0.0312 V/m compared to non-lesioned hemisphere E_{mean} = 0.8864 ± 0.0335 V/m, pair-wise *t*-test t(5) = 0.2041, p = 0.8463). Individual pair-wise *t*-tests for P1, P2, P4, and P6 indicated no statistical significant differences between the electric field strength of the lesioned and non-lesioned hemispheres (t(139) = 0.5968, p = 0.55; t(140) = 1.5188, p = 0.13; t(93) = -0.1946, p = 0.85; and t(126) = -1.2852, p = 0.20, respectively). P3 and P5 showed statistical significant differences in the electric field strength between hemispheres (t(20) = 5.5986, p = 6.9×10^{-8} and t(178) = 3.0784, p = 0.0024, respectively, p-value Bonferroni corrected for multiple comparisons p = 0.05/6 = 0.0083). These distributions

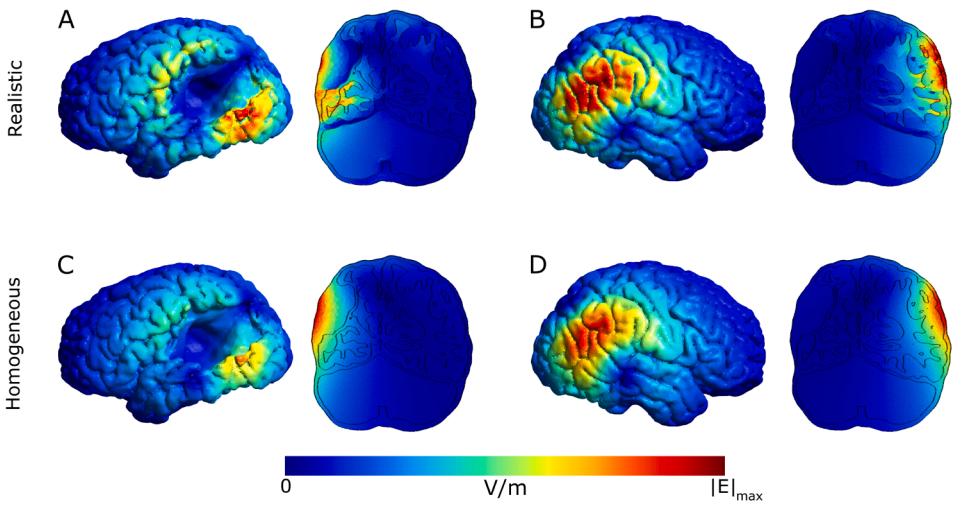

Fig. 3. Example electric field simulation results for a given TMS coil location over the lesion and its mirrored position over the non-lesioned hemisphere for both realistic and homogeneous conductivities. The coronal slices correspond to the plane going through the center of the coil. All figures (A-D) are scaled to the same maximum including the electric field strength in WM, GM and CSF. A) Realistic conductivity, over lesion position. The electric field strength maximum in GM is shifted to and enhanced at the bottom edge of the lesion. B) realistic conductivity, mirrored position. The electric field strength maximum in GM stays on the gyri near the coil center. C) homogeneous conductivity, over lesion position. The electric field strength is unaffected by the presence of a lesion and uniformly decays with distance from the coil center. D) homogeneous conductivity, mirrored position. The electric field strength is unaffected by the presence of gyri and uniformly decays with distance from the coil center.

were tested for normality using the one-sample Kolmogorov-Smirnov test.

However, we found that the coefficient of variation (standard deviation/mean) was larger for each individual's lesioned hemisphere compared to the non-lesioned hemisphere, indicating a larger spread in electric field strengths ($t(5) = 2.7724$, $p = 0.0393$). Across participants, the average coefficient of variation was 5.5% ± 1.3% (lesioned hemisphere) and 3.7% ±0.8% (non-lesioned hemisphere), or a 50% larger coefficient for the lesioned hemisphere. Individually, the lesioned hemisphere's coefficient of variation was 2% to 130% larger than the non-lesioned coefficient. The individual values can be found in Table 2.

To investigate the effects of a lesion on the induced electric field in further detail, we compared the simulation results at the individual level. We found that electric field strengths in GM were reduced for TMS coil locations directly above large cortical lesions (Fig. 4A, P1 + P2). In this case, electric field distributions differed most strongly between lesioned and non-lesioned hemispheres (Fig. 4B, P1 + P2). For small lesions (Fig. 4A + B, P4) no large differences in electric field strengths occurred. The coil positions that are included in the lesion group are directly over the lesion and their mirrored positions. Lesion positions are shown in the supplementary Figure S2. Simulation results for subcortical lesions are shown in Fig. 5. Correlation plots comparing results between hemispheres are also included in Figures S11 + S12 for cortical and subcortical lesions, respectively.

The shift in the location of the robust maximum (99.9th percentile) electric field is another measure that could be affected by the lesions. Figures S13 + S14 show how much the robust maximum shifts from directly under the center of the coil for each coil position. The lack of brain tissue in cortical lesions results in large shifts directly over the lesion volume. However, the median shifts over intact cortical tissue are as expected in all cases except for the lesioned hemisphere in P6, as seen in Table 3. The largest differences are seen in P2, P4, and P6. Their lesioned hemisphere median shifts are respectively 45%, 38%, and 119% larger than the non-lesioned hemispheres.

Table 2
Normalized electric field strength coefficient of variation.

ID	Lesioned Hemisphere	Non-lesioned Hemisphere
P1	6.43%	3.64%
P2	6.57%	3.27%
P3	5.98%	5.25%
P4	3.30%	2.94%
P5	4.08%	3.98%
P6	6.72%	2.93%

Analyses for the 25 mm coil, additional coil orientation, and perpendicular and tangential components of the electric field are included in the supplementary material, Figures S3 – S10. For the cortical lesion participants, the tangential component of the electric field (Figure S9) follows the same pattern as the electric field strength (Fig. 4), i.e. coil positions directly above large cortical lesions have reduced electric field strength. The perpendicular component of the electric field in cortical lesion participants (Figure S7) demonstrate a pattern that is peculiar to each individual. P1 shows a decreased electric field for the lesioned hemisphere, while P2 has slightly higher electric fields for the coil positions over the lesions and their mirrored counterparts. However, for both the perpendicular and tangential components, the spread of electric fields over the lesioned hemisphere is larger than for the non-lesioned hemisphere, comparable to the overall electric field strength (Fig. 4). For the subcortical lesion participants (Figures S8 + S10), the electric field strength is similar for both the lesioned and non-lesioned hemispheres, while the spread of electric field strength for the lesioned hemisphere is greater.

Overall, the results are similar to the analyses presented above.

3.2. Statistical analysis

We investigated four factors to explain the electric field simulation results: coil-to-cortex distance, average CSF depth under the center of the coil, CSF volume under the center of the coil, and local curvature around the center of the coil. We report the single factor linear model adjusted R^2 mean and standard deviation across the six participants for each factor in Table 4. We found that the coil-to-cortex factor resulted in the highest explained variance $R^2 = 0.46$. The local curvature was the second most important factor with $R^2 = 0.11$. Other factors had only small explanatory power of the electric field strength. Individual R^2 and p-values can be found in the supplementary table S1.

4. Discussion

Here, we performed TMS electric field simulations to evaluate the impact of brain lesions in six individuals with perinatal stroke. Our results are in line with previous work in adult stroke (Minjoli et al., 2017) highlighting a local influence of a lesion on the induced electric field. We expand this work to a pediatric population and investigate in detail the effects of cortical and subcortical lesions. Our investigation of different anatomical factors also goes beyond previous work (Wagner et al., 2006) and no direct comparison can be made between our findings. This can be explained by the limitations of that study: 1) At the time, the technical

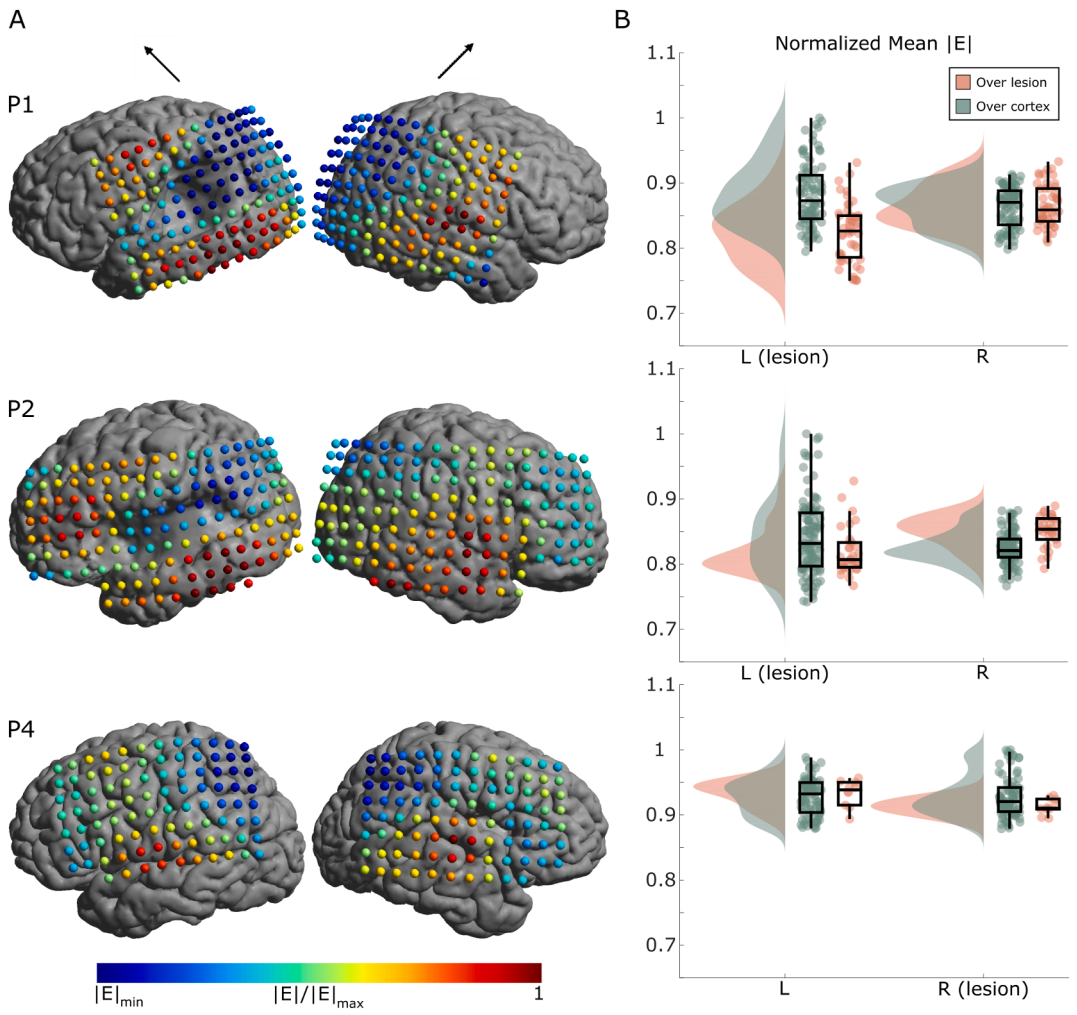

Fig. 4. Electric field simulation results for cortical lesion models (P1, P2, and P4). A) The normalized mean electric field strength in GM at each coil position for both left and right hemispheres (left and right columns, respectively). The black arrows above the columns indicate the coil orientation. The minimums are individualized for each participant (P1 $|E|_{min} = 0.7499$, P2 $|E|_{min} = 0.7419$, P4 $|E|_{min} = 0.8788$). For TMS coil positions directly above large cortical lesions the electric field strength is reduced. B) Raincloud plots (Allen et al., 2019) of the mean electric field strength over all stimulation locations. Orange dots indicate positions directly over the lesion (and equivalent positions over the non-lesioned hemisphere); green dots indicate positions over non-lesioned cortex. The spread of electric field strength over the lesioned hemisphere is larger than for the non-lesioned hemisphere. (For interpretation of the references to colour in this figure legend, the reader is referred to the web version of this article.)

capabilities of TMS computational modeling were not advanced enough to capture the realistic head morphologies. (Wagner et al., 2006) modeled the brain as a flat surface, discarding the gyrification of the brain, and also did not model the white matter. 2) (Wagner et al., 2006) studied the alteration in the distribution of TMS-induced current densities as a result of brain lesions, rather than the electric field intensity. While we found no difference on average electric field strengths between lesioned and non-lesioned hemispheres, there was larger variability in the lesioned hemisphere. We observed the most profound effect on electric field variability for cortical lesions whereas lesioned and non-lesioned hemispheres were more similar for subcortical lesions. This is not surprising given that TMS mostly affects superficial brain regions where the interface between GM-CSF has an important influence on the TMS electric field. On the other hand, we found that coil-to-cortex distance has a strong influence on the TMS electric field for both lesioned and non-lesioned hemispheres.

A pulse from a TMS coil directly above a large lesion will shift the maximum electric field strength to neighboring gyri. However, the changes in the TMS electric fields caused by lesions are not easily captured by a homogeneous model or through simple local measures such as CSF thickness, curvature or volume. This indicates the need for individualized and realistic modeling to guide practical applications of TMS in stroke rehabilitation to capture idiosyncrasies, e.g., variations in morphology and resultant anatomy.

Our study has some limitations. First, we assign conductivity values based on literature values (Windhoff et al., 2013). However, these conductivity values can differ amongst individuals (Saturnino et al., 2019), so they will be difficult to predict in the pediatric brain undergoing various brain development processes affecting both GM and WM (Brain Development Cooperative Group, 2012). Further, we assumed the lesions were CSF-filled volumes, similar to both (Wagner et al., 2006) and (Minjoli et al., 2017). However, amongst CSF, glial scarring and other inactive tissues will fill the lesion space, which could also affect the conductivity of the region. Nevertheless, we do not expect these points to strongly affect our simulation results as TMS electric fields are robust to uncertainties in GM and CSF tissue conductivities which most strongly affected the electric field strength (Saturnino et al., 2019; Thielscher et al., 2011). The large conductivity difference between these two tissue types means that small deviations within each tissue type have a small effect on the induced electric field.

In addition, we worked with a limited sample size with large variability in lesion size and location. Future improvements in automating

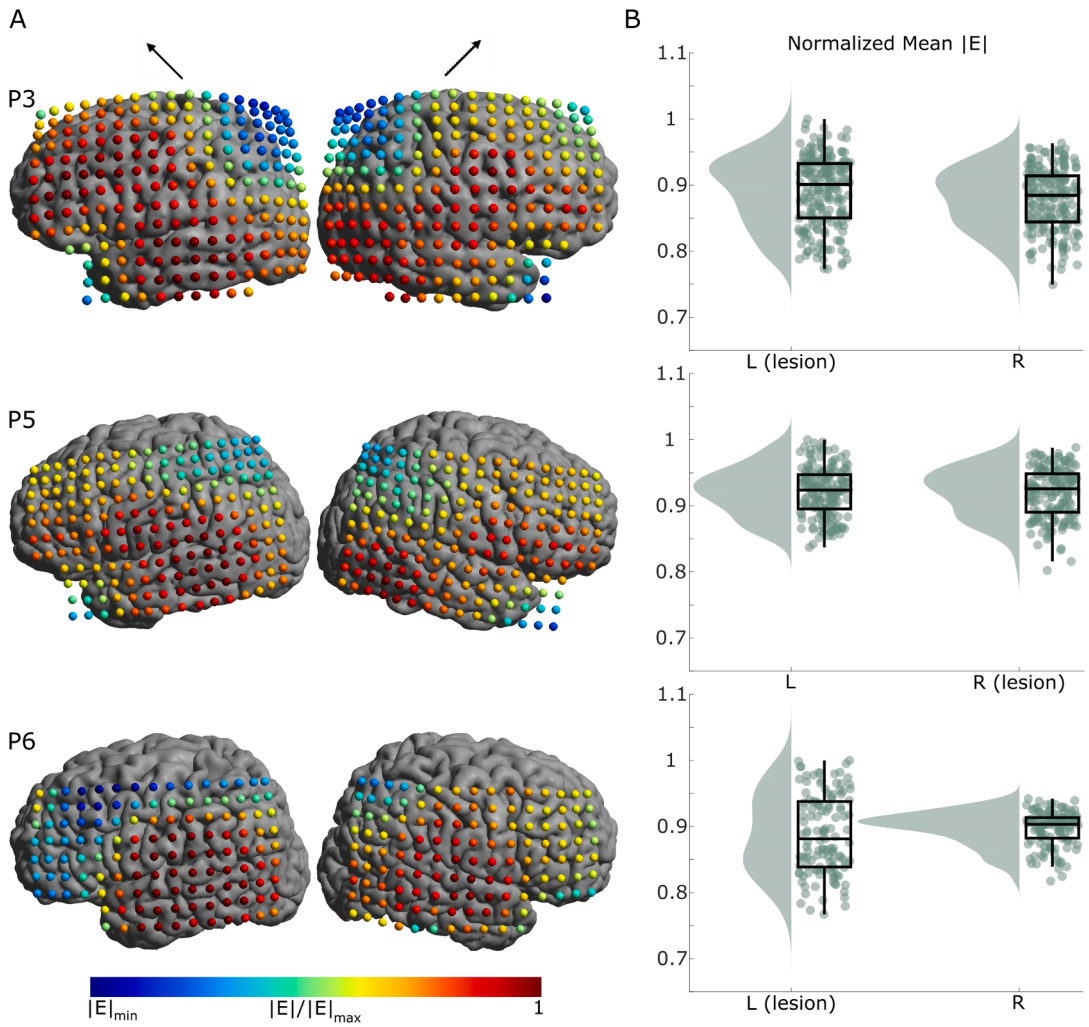

Fig. 5. Electric field simulation results for subcortical lesion models (P3, P5, and P6). A) The mean electric field strength in GM at each coil position for both left and right hemispheres (left and right columns, respectively). The black arrows above the columns indicate the coil orientation. The minimums are individualized for each participant (P3 $|E|_{min} = 0.7494$, P5 $|E|_{min} = 0.8022$, P6 $|E|_{min} = 0.7671$). The electric field strength is similar for both the lesioned and non-lesioned hemispheres B) Raincloud plots (Allen et al., 2019) of the mean electric field strength over all stimulation locations. The spread of electric field strength for the lesioned hemisphere is greater despite the lesion being subcortical.

Table 3
Robust maximum electric field shift distance from directly under the coil center (mean ± std, median).

	Lesioned hemisphere	Non-lesioned hemisphere
P1	4.06 ± 2.49 mm, 3.69 mm	4.14 ± 2.61 mm, 3.67 mm
P2	6.67 ± 4.20 mm, 5.64 mm	4.26 ± 2.38 mm, 3.89 mm
P3	4.68 ± 3.03 mm, 4.23 mm	4.93 ± 3.47 mm, 3.90 mm
P4	4.70 ± 2.28 mm, 4.36 mm	3.50 ± 1.80 mm, 3.15 mm
P5	4.57 ± 3.14 mm, 3.65 mm	4.38 ± 2.39 mm, 3.87 mm
P6	8.56 ± 6.36 mm, 7.04 mm	3.80 ± 2.72 mm, 3.21 mm

Table 4
Adjusted R^2 values of single factor linear model results for both lesioned and non-lesioned hemispheres. Reported are mean ± std across participants.

Factor	Adjusted R^2 Lesioned Hemisphere	Adjusted R^2 Non-Lesioned Hemisphere
Coil-to-cortex distance (mm)	0.4623 ± 0.1312	0.4452 ± 0.1790
CSF depth (mm)	0.0681 ± 0.0979	0.1274 ± 0.1149
CSF volume (mm^3)	0.0697 ± 0.0729	0.0647 ± 0.0378
Local curvature	0.1085 ± 0.0946	0.2123 ± 0.1406

model generation will reduce the significant effort in model creation and facilitate the application of modeling in larger populations. Nevertheless, we could identify similar changes in electric field strengths in participants with large cortical lesions compared to individuals with small cortical or predominantly subcortical lesions.

Recent computational and experimental work highlights the complexity in accurately and effectively stimulating target networks with TMS. Technical factors ranging from coil placement and orientation to pulse duration impact which neurons are affected by TMS (Aberra et al., 2020; Gomez–Tames et al., 2020; Goodwin and Butson, 2015; Hannah and Rothwell, 2017; Laakso et al., 2018). Individual differences in brain morphology, particularly in brain regions with high structural variability, exacerbate challenges of TMS targeting (Gomez-Tames et al., 2018). Combining these previous efforts with the modeling work presented here has the potential to guide TMS targeting and dosing for treatment and rehabilitation in pediatric stroke.

5. Conclusion

Lesions increase the variability of the electric field strength, depending on lesion size and whether it is cortical or subcortical. The results suggest that coil placement strategies have to be carefully

considered in the presence of a lesion due to an increased variability in electric field strength. Therefore, our individualized modeling framework can be instrumental for accurately applying TMS for stroke rehabilitation in both adult and pediatric populations. Future work will include comparing TMS simulation results to experimental MEP data to validate model accuracy in the presence of lesions. This can be used to optimize TMS coil positioning based on a model driven approach (Weise et al., 2020) to stimulate specific brain areas for stroke rehabilitation.

CRediT authorship contribution statement

Kathleen E. Mantell: Conceptualization, Data acquisition, Formal analysis, Investigation, Methodology, Visualization, Writing – original draft, Writing – review & editing. **Ellen N. Sutter:** Data acquisition, Writing – original draft, Writing – review & editing. **Sina Shirinpour:** Formal analysis, Writing – review & editing. **Samuel T. Nemanich:** Data acquisition, Writing – original draft, Writing – review & editing. **Daniel H. Lench:** Data acquisition, Writing – original draft, Writing – review & editing. **Bernadette T. Gillick:** Conceptualization, Supervision, Funding acquisition. **Alexander Opitz:** Conceptualization, Supervision, Writing – original draft, Writing – review & editing, Funding acquisition

Declaration of Competing Interest

The authors declare that they have no known competing financial interests or personal relationships that could have appeared to influence the work reported in this paper.

Acknowledgments

Research presented here was supported by the University of Minnesota's MnDRIVE Initiative, National Institutes of Health R21HD097575 and RF1MH117428, and the Shepherd Trust/Jensen Family.

Appendix A. Supplementary data

Supplementary data to this article can be found online at https://doi.org/10.1016/j.nicl.2021.102563.

References

Aberra, A.S., Wang, B., Grill, W.M., Peterchev, A.V., 2020. Simulation of transcranial magnetic stimulation in head model with morphologically-realistic cortical neurons. Brain Stimulation 13 (1), 175–189. https://doi.org/10.1016/j.brs.2019.10.002.

Agrawal, N., Johnston, S.C., Wu, Y.W., Sidney, S., Fullerton, H.J., 2009. Imaging Data Reveal a Higher Pediatric Stroke Incidence Than Prior US Estimates. Stroke 40 (11), 3415–3421. https://doi.org/10.1161/STROKEAHA.109.564633.

Alekseichuk, I., Mantell, K., Shirinpour, S., Opitz, A., 2019. Comparative modeling of transcranial magnetic and electric stimulation in mouse, monkey, and human. NeuroImage 194, 136–148. https://doi.org/10.1016/j.neuroimage.2019.03.044.

Allen, M., Poggiali, D., Whitaker, K., Marshall, T.R., Kievit, R.A., 2019. Raincloud plots: a multi-platform tool for robust data visualization. Wellcome Open Res 4, 63. https://doi.org/10.12688/wellcomeopenres.15191.1.

Attene, M., 2010. A lightweight approach to repairing digitized polygon meshes. Vis Comput 26 (11), 1393–1406. https://doi.org/10.1007/s00371-010-0416-3.

Brain Development Cooperative Group, 2012. Total and Regional Brain Volumes in a Population-Based Normative Sample from 4 to 18 Years: The NIH MRI Study of Normal Brain Development. Cereb Cortex 22, 1–12. https://doi.org/10.1093/cercor/bhr018.

Bungert, A., Antunes, A., Espenhahn, S., Thielscher, A., 2016. Where does TMS Stimulate the Motor Cortex? Combining Electrophysiological Measurements and Realistic Field Estimates to Reveal the Affected Cortex Position. Cereb. Cortex. https://doi.org/10.1093/cercor/bhw292.

Deng, Z.-D., Lisanby, S.H., Peterchev, A.V., 2013. Electric field depth–focality tradeoff in transcranial magnetic stimulation: Simulation comparison of 50 coil designs. Brain Stimulation 6 (1), 1–13. https://doi.org/10.1016/j.brs.2012.02.005.

Dionísio, A., Duarte, I.C., Patrício, M., Castelo-Branco, M., 2018. The Use of Repetitive Transcranial Magnetic Stimulation for Stroke Rehabilitation: A Systematic Review. J. Stroke Cerebrovascular Diseases 27 (1), 1–31. https://doi.org/10.1016/j.jstrokecerebrovasdis.2017.09.008.

Emara, T.H., Moustafa, R.R., ElNahas, N.M., ElGanzoury, A.M., Abdo, T.A., Mohamed, S. A., ElEtribi, M.A., 2010. Repetitive transcranial magnetic stimulation at 1Hz and 5Hz produces sustained improvement in motor function and disability after ischaemic stroke. European Journal of Neurology 17, 1203–1209. https://doi.org/10.1111/j.1468-1331.2010.03000.x.

Fischl, B., 2012. FreeSurfer. NeuroImage 62 (2), 774–781. https://doi.org/10.1016/j.neuroimage.2012.01.021.

Gillick, B., Rich, T., Nemanich, S., Chen, C.-Y., Menk, J., Mueller, B., Chen, M.o., Ward, M., Meekins, G., Feyma, T., Krach, L., Rudser, K., 2018. Transcranial direct current stimulation and constraint-induced therapy in cerebral palsy: A randomized, blinded, sham-controlled clinical trial. Eur. J. Paediatric Neurol. 22 (3), 358–368. https://doi.org/10.1016/j.ejpn.2018.02.001.

Gillick, B.T., Krach, L.E., Feyma, T., Rich, T.L., Moberg, K., Thomas, W., Cassidy, J.M., Menk, J., Carey, J.R., 2014. Primed low-frequency repetitive transcranial magnetic stimulation and constraint-induced movement therapy in pediatric hemiparesis: a randomized controlled trial. Dev. Med. Child Neurol. 56 (1), 44–52. https://doi.org/10.1111/dmcn.12243.

Gomez-Tames, J., Hamasaka, A., Laakso, I., Hirata, A., Ugawa, Y., 2018. Atlas of optimal coil orientation and position for TMS: A computational study. Brain Stimulation 11 (4), 839–848. https://doi.org/10.1016/j.brs.2018.04.011.

Gomez-Tames, J., Laakso, I., Murakami, T., Ugawa, Y., Hirata, A., 2020. TMS activation site estimation using multiscale realistic head models. Journal of Neural Engineering. https://doi.org/10.1088/1741-2552/ab8ccf.

Goodwin, B.D., Butson, C.R., 2015. Subject-Specific Multiscale Modeling to Investigate Effects of Transcranial Magnetic Stimulation: Subject-specific multiscale modeling of TMS. Neuromodulation: Technology at the Neural Interface 18 (8), 694–704. https://doi.org/10.1111/ner.12296.

Hannah, R., Rothwell, J.C., 2017. Pulse Duration as Well as Current Direction Determines the Specificity of Transcranial Magnetic Stimulation of Motor Cortex during Contraction. Brain Stimulation 10 (1), 106–115. https://doi.org/10.1016/j.brs.2016.09.008.

Hoyer, E.H., Celnik, P.A., 2011. Understanding and enhancing motor recovery after stroke using transcranial magnetic stimulation. Restorative Neurology and Neuroscience 29, 395–409. https://doi.org/10.3233/RNN-2011-0611.

Jenkinson, M., Beckmann, C.F., Behrens, T.E.J., Woolrich, M.W., Smith, S.M., 2012. FSL. NeuroImage 62 (2), 782–790. https://doi.org/10.1016/j.neuroimage.2011.09.015.

Kirton, A., Chen, R., Friefeld, S., Gunraj, C., Pontigon, A.-M., deVeber, G., 2008. Contralesional repetitive transcranial magnetic stimulation for chronic hemiparesis in subcortical paediatric stroke: a randomised trial. Lancet Neurol. 7 (6), 507–513. https://doi.org/10.1016/S1474-4422(08)70096-6.

Laakso, I., Murakami, T., Hirata, A., Ugawa, Y., 2018. Where and what TMS activates: Experiments and modeling. Brain Stimulation 11 (1), 166–174. https://doi.org/10.1016/j.brs.2017.09.011.

Lindenberg, R., Renga, V., Zhu, L.L., Nair, D., Schlaug, G., 2010. Bihemispheric brain stimulation facilitates motor recovery in chronic stroke patients. Neurology 75 (24), 2176–2184. https://doi.org/10.1212/WNL.0b013e318202013a.

Malcolm, M.P., Triggs, W.J., Light, K.E., Gonzalez Rothi, L.J., Wu, S., Reid, K., Nadeau, S. E., 2007. Repetitive Transcranial Magnetic Stimulation as an Adjunct to Constraint-Induced Therapy: An Exploratory Randomized Controlled Trial. Am. J. Phys. Med. Rehabil. 86 (9), 707–715. https://doi.org/10.1097/PHM.0b013e31813e0de0.

Minjoli, S., Saturnino, G.B., Blicher, J.U., Stagg, C.J., Siebner, H.R., Antunes, A., Thielscher, A., 2017. The impact of large structural brain changes in chronic stroke patients on the electric field caused by transcranial brain stimulation. NeuroImage: Clinical 15, 106–117. https://doi.org/10.1016/j.nicl.2017.04.014.

Miranda, P.C., Hallett, M., Basser, P.J., 2003. The electric field induced in the brain by magnetic stimulation: a 3-d finite-element analysis of the effect of tissue heterogeneity and anisotropy. IEEE Trans. Biomed. Eng. 50 (9), 1074–1085. https://doi.org/10.1109/TBME.2003.816079.

Nielsen, J.D., Madsen, K.H., Puonti, O., Siebner, H.R., Bauer, C., Madsen, C.G., Saturnino, G.B., Thielscher, A., 2018. Automatic skull segmentation from MR images for realistic volume conductor models of the head: Assessment of the state-of-the-art. NeuroImage 174, 587–598. https://doi.org/10.1016/j.neuroimage.2018.03.001.

Opitz, A., Fox, M.D., Craddock, R.C., Colcombe, S., Milham, M.P., 2016. An integrated framework for targeting functional networks via transcranial magnetic stimulation. NeuroImage 127, 86–96. https://doi.org/10.1016/j.neuroimage.2015.11.040.

Opitz, A., Legon, W., Rowlands, A., Bickel, W.K., Paulus, W., Tyler, W.J., 2013. Physiological observations validate finite element models for estimating subject-specific electric field distributions induced by transcranial magnetic stimulation of the human motor cortex. NeuroImage 81, 253–264. https://doi.org/10.1016/j.neuroimage.2013.04.067.

Opitz, A., Windhoff, M., Heidemann, R.M., Turner, R., Thielscher, A., 2011. How the brain tissue shapes the electric field induced by transcranial magnetic stimulation. NeuroImage 58 (3), 849–859. https://doi.org/10.1016/j.neuroimage.2011.06.069.

Opitz, A., Zafar, N., Bockermann, V., Rohde, V., Paulus, W., 2014. Validating computationally predicted TMS stimulation areas using direct electrical stimulation in patients with brain tumors near precentral regions. NeuroImage: Clinical 4, 500–507. https://doi.org/10.1016/j.nicl.2014.03.004.

Ridding, M.C., Rothwell, J.C., 2007. Is there a future for therapeutic use of transcranial magnetic stimulation? Nat Rev Neurosci 8 (7), 559–567. https://doi.org/10.1038/nrn2169.

Rossi, S., Hallett, M., Rossini, P.M., Pascual-Leone, A., 2009. Safety, ethical considerations, and application guidelines for the use of transcranial magnetic stimulation in clinical practice and research. Clin. Neurophysiol. 120 (12), 2008–2039. https://doi.org/10.1016/j.clinph.2009.08.016.

Saturnino, G.B., Thielscher, A., Madsen, K.H., Knösche, T.R., Weise, K., 2019. A principled approach to conductivity uncertainty analysis in electric field

calculations. NeuroImage 188, 821–834. https://doi.org/10.1016/j.neuroimage.2018.12.053.
Theilig, S., Podubecka, J., Bösl, K., Wiederer, R., Nowak, D.A., 2011. Functional neuromuscular stimulation to improve severe hand dysfunction after stroke: Does inhibitory rTMS enhance therapeutic efficiency? Exp. Neurol. 230 (1), 149–155. https://doi.org/10.1016/j.expneurol.2011.04.010.
Thielscher, A., Opitz, A., Windhoff, M., 2011. Impact of the gyral geometry on the electric field induced by transcranial magnetic stimulation. NeuroImage 54 (1), 234–243. https://doi.org/10.1016/j.neuroimage.2010.07.061.
Wagner, T., Fregni, F., Eden, U., Ramos-Estebanez, C., Grodzinsky, A., Zahn, M., Pascual-Leone, A., 2006. Transcranial magnetic stimulation and stroke: A computer-based human model study. NeuroImage 30 (3), 857–870. https://doi.org/10.1016/j.neuroimage.2005.04.046.
Weise, K., Numssen, O., Thielscher, A., Hartwigsen, G., Knösche, T.R., 2020. A novel approach to localize cortical TMS effects. NeuroImage 209, 116486. https://doi.org/10.1016/j.neuroimage.2019.116486.
Wiethoff, S., Hamada, M., Rothwell, J.C., 2014. Variability in Response to Transcranial Direct Current Stimulation of the Motor Cortex. Brain Stimulation 7 (3), 468–475. https://doi.org/10.1016/j.brs.2014.02.003.
Windhoff, M., Opitz, A., Thielscher, A., 2013. Electric field calculations in brain stimulation based on finite elements: An optimized processing pipeline for the generation and usage of accurate individual head models. Hum. Brain Mapp. 34 (4), 923–935. https://doi.org/10.1002/hbm.21479.
Yushkevich, P.A., Piven, J., Hazlett, H.C., Smith, R.G., Ho, S., Gee, J.C., Gerig, G., 2006. User-guided 3D active contour segmentation of anatomical structures: Significantly improved efficiency and reliability. NeuroImage 31 (3), 1116–1128. https://doi.org/10.1016/j.neuroimage.2006.01.015.